Proposal and design of short armature core double-sided transverse flux type linear synchronous motor

Shin Jung-Seob[1], *Student Member, IEEE,* Takafumi Koseki[1], *Member, IEEE* and Kim Houng-Joong[2]

[1]The University of Tokyo, Engineering Building #2 12F, 7-3-1 Hongo, Bunkyo-ku, Tokyo 113-8656, Japan
[2]Sung-Jin Royal Motion Co. Ltd, 987-4, Gosaek-dong, Gwonseon-gu, Suwon, Gyeonggi-do, 441-813, Korea

In this paper, the authors propose short armature core double-sided transverse flux type linear synchronous motor. First, the operational principle and structural advantages of the proposed model are introduced. Focusing on one-core based configuration, a theoretical design of thrust in the designated dimension is then conducted for a simple estimation in the preliminary design stage. Finally, thrust is analyzed and evaluated through field calculations using 3-D finite element method.

***Index Terms*— High thrust, permanent magnet linear synchronous motor (PMLSM), transverse flux machinery (TFM).**

I. Introduction

LINEAR MOTORS are increasingly employed in industrial fields. There are many types of linear motors, including linear synchronous, linear induction, and linear stepping motors. Especially, the permanent magnet linear synchronous motor (PMLSM) has contributed to the popularization of linear motors in industrial fields with the advent of rare earth magnet.

High thrust density is an important technical performance requirement for PMLSMs. The transverse flux type machinery (TFM) is an ideal alternative [1]. However, conventional TFM has a relatively complex structure that requires relatively large manufacturing effort [2].

The authors propose short armature core double-sided transverse flux type linear synchronous motor for high thrust.

In this paper, the operational principle and structural advantages of the proposed model are introduced in Section II. In Section III, focusing on a one-core based configuration, a theoretical design of thrust in the designated dimension is conducted for a simple estimation. Finally, in Section IV, thrust is analyzed and evaluated through field calculations using the 3-D finite element method (FEM). The JMAG-Designer 10.4.3h commercial package was used for the 3-D FEM analysis.

II. Basic Structure and Operational Principles

In the PMLSM development stage, structural concept is one of the most important factors with the optimal design. The authors focused on the following in the development stage.

(a) Easy assembly and manufacturing

It will be achieved by fabricating an iron core with laminated steel plates and easy winding work.

(b) Flux leakage reduction for high thrust

Placing field magnets on the field core surface and having a short air gap length could reduce flux leakage. In addition, the magnetic flux linking an armature coil will be reduced slightly by having the armature coils closed to the field magnet.

(c) Double-sided structure

A double-sided structure is useful in compensating for the strong normal attractive force between the armature and the field side.

Fig. 1 shows the fundamental configuration of a three-phase unit of the proposed model.

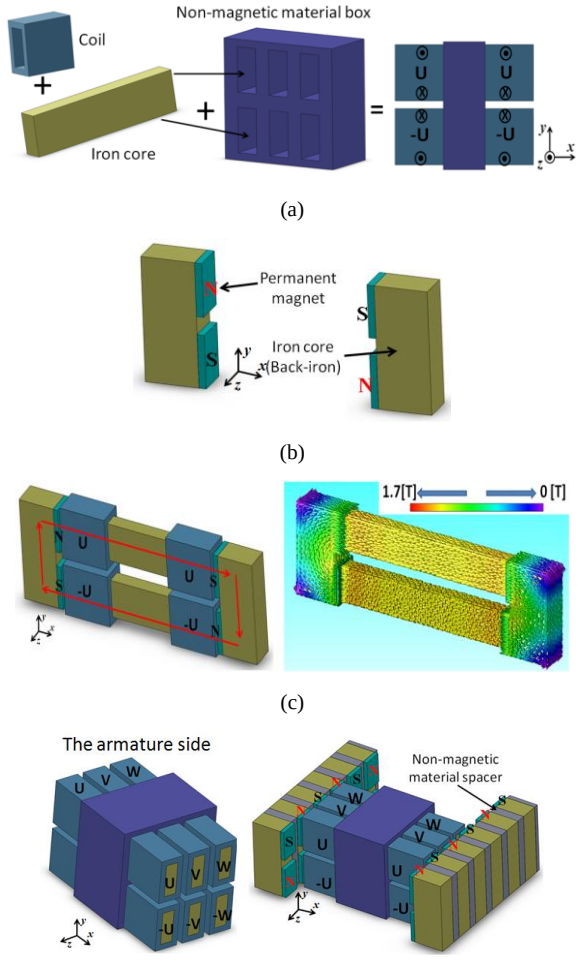

Fig. 1. Fundamental configuration of the three-phase unit. (In (c), the red arrows denote flux flow; the non-magnetic material box was removed for easy understanding.) (a) An armature unit (mover). (b) A field unit (stator). (c) A magnetic circuit. (d) Configuration along the moving direction.

An armature unit can be assembled by inserting two square-shaped iron cores into a non-magnetic material box, as shown

Manuscript received March 2, 2012. Corresponding author: Shin Jung-Seob (e-mail: jungseobshin1008@koseki.t.u-tokyo.ac.jp).
Digital Object Identifier inserted by IEEE

in Fig. 1(a). A field unit consists of four magnets, a square-shape iron core as back-iron on both sides, as shown in Fig. 1 (b).

Inserting an armature core into the non-magnetic material box creates two salient poles on both sides. The armature coils are then inserted on each salient pole.

The square-shaped iron core employed in the armature and field side can be easily fabricated using a laminated steel plate that is arranged along the *z* direction.

A magnetic circuit comprises an inserted armature unit and a field unit, as shown in Fig. 1 (c). Flux from the north pole flows into the south pole along the short armature core. Two coils in the lower side are wound in a direction opposite to the two coils in the upper side, and these coils are connected in series. By adding current to these coils, they are excited with 180-phase difference.

The armature cores are arranged along the moving direction *z*, as shown in Fig. 1 (d). Each armature core is spatially separated by 120 degrees difference. The field magnets are arranged along the moving direction *z* with a non-magnetic spacer, and each magnet is electrically separated by 180 degrees. The non-magnetic material spacer isolates the magnetic paths.

By adding AC current which has 120-degree phase differences to each armature coil, the proposed model operates as a three-phase AC synchronous motor. Here, -U, -V, and -W are the current components shifted 180 degrees from U,V, and W.

III. Theoretical Design of Thrust for Simple Estimation

In a theoretical design for a simple estimation, the authors have focused on the thrust behavior in a one-core based configuration. This is because the thrust behavior in a three-phase configuration can be estimated by superposing the results of the one-phase configuration.

Variables employed in the preliminary design are shown in Fig. 2. Since detent force can be reduced by applying core-pole combination, the authors have considered a 9 core-8 pole combination and chose 100 × 40 × 108 mm^3 as the total dimension [3]. Specifications of the design are shown in Table I.

In creating a theoretical design of thrust, the authors focused on l_a defined in Fig. 2(b). Geometrically, the larger l_a is, the higher the winding turn per armature pole can be achieved. It represents the increase of electrical load by increasing the magnetomotive force (MMF). In addition, the authors considered the magnet length in the magnetization direction l_m to be 5.4 mm, which is the initial design area.

With a variation of l_a, the dimensions of the armature core in each axis l_x, l_y, and l_z are expressed as (1). Also, dimensions in the cross-section of the armature core and space for the armature winding are expressed as (2).

$$l_x = 2(L_a - l_f - l_m - l_g), \quad l_y(l_a) = 0.5L_a - 2l_a = 2(b - l_a),$$
$$l_z(l_a) = \tau_s - 2l_a = 2(a - l_a) \tag{1}$$

$$A_a(l_a) = l_y(l_a) \times l_z(l_a), \quad A_w(l_a) = l_a \times l_c \tag{2}$$

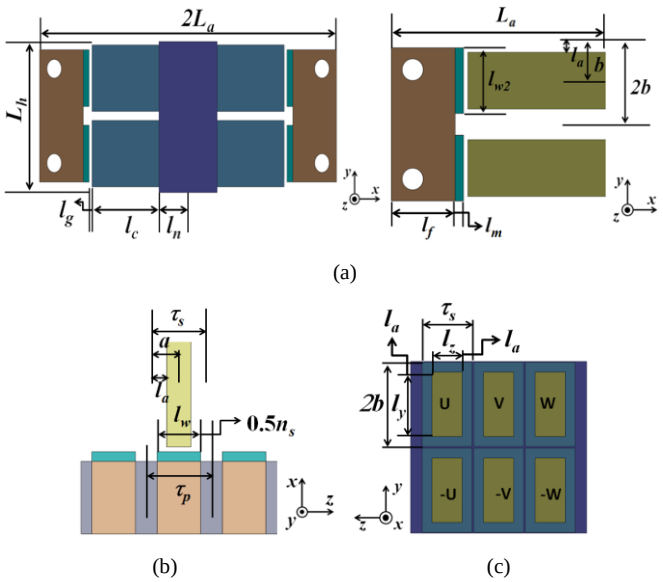

Fig. 2. Variables employed in the preliminary design (In (a) and (b), the armature coils are removed for clarity. Also, variables are labeled in the half side because of symmetric structure.). (a) x-y plain. (b) x-z plain. (c) y-z plain.

TABLE I
DESIGN SPECIFICATIONS IN THE PROPOSED MODEL

Symbol	Quantity	Note
L_a	50 [mm]	Half-length in cross-section
L_h	40 [mm]	Height in cross-section
τ_p	13.5 [mm]	Pole pitch
τ_s	12 [mm]	Slot pitch
l_w	9 [mm]	Magnet length to z-direction
l_{w2}	15 [mm]	Magnet length to y-direction
l_f	15 [mm]	Back yoke length to x-direction
l_n	10 [mm]	Half-length of non-magnetic material box
n_s	4.5 [mm]	Length of non-magnetic spacer
a	6 [mm]	Half-length of core pitch
b	10 [mm]	Half-length of height
l_c	19.6 [mm]	Half-length of core pitch
l_g	1 [mm]	Mechanical air gap length
l_a	Variable	Half-length of slot

For a theoretical derivation of thrust, the authors employed a magnetic circuit method and made the following fundamental assumptions for a simple estimation [4]-[5]. To achieve a precise estimation, the flux path and its distribution in the air gap would be required.

(a) The air gap flux density B_g is the same as the magnet flux density B_m and its distribution is constant regardless of the slot effect.

(b) In the calculation of B_m, the air gap length l_{gc} applied Carter coefficient is used to compensate for the slot effect.

(c) Permeability of the iron cores are infinitely large.

From these assumptions and Fig. 1(c), a magnetic circuit of the proposed model can be expressed as

$$H_m l_m + H_g l_{gc} = H_m l_m + R_g \phi_g = 0 \tag{3}$$

where H_m and H_g are the magnetic-field component of the magnet and the air gap, respectively, R_g is the magnetic reluctance in the air gap and ϕ_g is the air gap flux. From (3), H_m can be expressed as (4). In (4), μ_0 is the permeability of air.

$$H_m = -\frac{B_m l_{gc}}{\mu_0 l_m} \tag{4}$$

Here, B_m in operating point is (5). B_r is remanence of the field magnet. By substituting (4) into (5), B_m under a no-load condition can be expressed as (6).

$$B_m = B_r + \mu_0 H_m \tag{5}$$

$$B_m = B_g = B_r \Big/ \left(1 + \frac{l_{gc}}{l_m}\right) \tag{6}$$

Also, the authors assume that the flux flowing from the field magnet to the armature core is defined as ϕ_a and is determined by (7).

$$\phi_a = B_m \times A_a \tag{7}$$

This means that the flux density in the armature core is the same as B_m and the flux in the space where the armature does not faced the field magnet does not contribute to thrust. If ϕ_a by moving an armature unit is modeled as shown in Fig. 3, it can be expressed as Fourier series. Its fundamental component is (8). In (8), z is the distance in the moving direction and can be expressed by velocity v multiplied by time t.

$$\phi_a(z, l_a) = \frac{4B_m A_a(l_a)}{\pi} \sin\left(\frac{\pi(a - l_a)}{\tau_p}\right) \cos\left(\frac{\pi z}{\tau_p}\right) \tag{8}$$

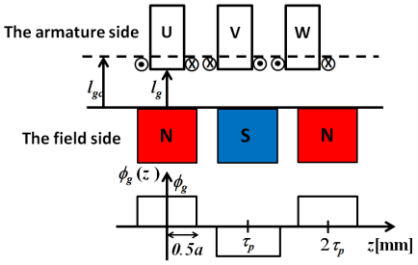

Fig. 3. Effective flux distribution resulting from moving an armature unit.

The authors assumed that all the $\phi_a(z,l_a)$ are linked to an armature coil. Hence, the flux linking to an armature coil $\phi_c(z,l_a)$ is the same as $\phi_a(z,l_a)$.

From (8), it is found that $\phi_c(z,l_a)$ becomes zero when l_a is equal to a because the armature core does not exist. This reflects that the flux from the field magnet does not link to the armature coil and flows into the field magnets which have the south pole in the moving direction even though an armature coil actually exists. This is due to the inherent characteristic of permanent magnet that flux from the north pole tends to flow to the south pole along the shortest path.

When l_a is equal to zero, it has to be zero because it is the same as the slot-less condition in which all the armature cores are attached to each other along the moving direction. However, it is not zero. This characteristic is compensated for by a coefficient defined in (9).

$$k_c(l_a) = \frac{A_a(0) - A_a(l_a)}{A_a(l_a)} \tag{9}$$

The back electromotive force (EMF) can be expressed as (10). In (10), $N(l_a,l_c)$ is the number of winding turns on a salient pole.

$$E(z) = -k_c(l_a) N(l_a, l_c) \frac{d\phi_c(z, l_a)}{dt} \tag{10}$$

Thrust per armature unit is considered the fundamental component in Fourier series and can be expressed as (11). In (11), P is electromagnetic power, E_{rms} is the RMS value of the back EMF, p is the number of poles in a field unit, and $\alpha(l_a,l_c)$ is the lamination factor of the coil. Also, $A_w(l_a,l_c)$ is the dimension of the cross-section in which the armature coil is wound, I is armature current, and S_c and J are the dimension of a conductor and current density, respectively.

From (11), thrust is generally determined by electrical load multiplied by magnetic load when other conditions, including armature current, and pole pitch are constant. Electrical load means MMF $N(l_a,l_c)I$ and is spatially determined by l_a and l_c. Magnetic load means B_m and is also spatially determined by l_m when the air gap is constant.

$$F_t(l_a) = p\frac{P_{out}}{v} = p\frac{E_{rms} I}{v} = \frac{2\sqrt{2} p k_c(l_a) B_m A_a(l_a) N(l_a,l_c) I}{\tau_p} \sin\left(\frac{\pi(a - l_a)}{\tau_p}\right)$$
$$\left(\therefore N(l_a,l_c) I = \frac{\alpha(l_a,l_c) A_w(l_a,l_c) I}{S_c} = \alpha(l_a,l_c) A_w(l_a,l_c) J\right) \tag{11}$$

IV. Analysis and Evaluation

To analyze thrust, the authors applied 3-D FEM field analysis to the proposed model. The specifications and result in the initial design area are shown in Table II and Fig. 4.

TABLE II
Specifications in Analysis

Symbol	Quantity	Symbol	Quantity
J	7 [A/mm^2]	I	3.4 [A]
S_c	0.804 × 0.804 [mm] (conductor: 0.7 × 0.7)	p	4
v	1 [m/s]	B_r	1.32 [T]

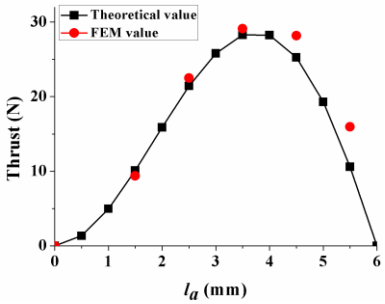

Fig. 4. Thrust in the initial design area.

In a rated area, the maximum thrust in the initial design area was at 3.5 mm and the error between theoretical values and FEM values was small. In this point, the armature core width

along the moving direction was 5 mm.

Thrust decreases from 3.5 mm because of the decreasing flux linkage to the armature coil, regardless of spatially increased MMF. However, the errors between theoretical values and FEM values increased. This is due to the Carter coefficient used to compensate for the slot effect. The larger the ratio between the slot width and slot pitch, the larger an increase ratio of the Carter coefficient is, which results in a decrease of B_m. This is more significant in case of larger slot width [4]. For that reason, the air gap flux density is smaller than expected and the theoretical thrust becomes lower than the FEM value.

The authors decided on l_a=3.5 mm as the point at which high thrust could be obtained in the initial design area.

However, from the result of detent force and its ratio of detent force to thrust based on the 3-D FEM result, the overall detent force was larger than thrust in the initial design area, as shown in Fig. 5.

This means the magnetic load affected by the field magnet was larger than the electrical load affected by the MMF. Generally, a large magnetic load can cause a large detent force, thrust ripple, or vibration, which can result in a poor performance.

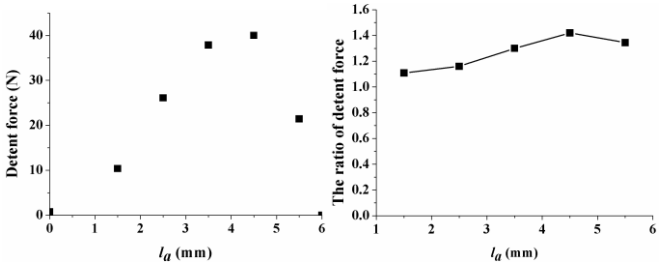

(a) (b)

Fig. 5. Detent force and its ratio to thrust in the initial design area. (a) Detent force. (b) Ratio of detent force to thrust.

Thus, it is important to find the point at which high thrust and low detent force can be achieved. The authors evaluated this aspect using the ratio of detent force to thrust. Fig. 6 shows the results of thrust, detent force, and the ratio of detent force to thrust at various l_m. The authors did not consider l_m=1 mm because of the difficulty of magnet fabrication.

From Fig. 6(a), it was found that the maximum thrust was at l_a=3.5 mm for all values of l_m. Also, there was a similar tendency when comparing the results in Fig. 6(a) and (b).

In particular, when l_m increased from 4 mm to 5.4 mm, increase of thrust was small, as shown in Fig. 6 (a) and (b). This was due to spatial limitations in the proposed model. When l_m varies from 4 mm to 5.4 mm, a decrease ratio of *NI* (7.6%) is larger than an increase ratio of B_m (7.3%), which results in a decrease of thrust at 5.4 mm.

From the results in Fig. 6(c), the ratio of detent force was improved with a decrease of l_m and less than one in l_m=2 mm. When considering a design for high thrust and low detent force within a designated dimension, a good point for further optimal design was in l_m=2 mm and l_a=3.5 mm.

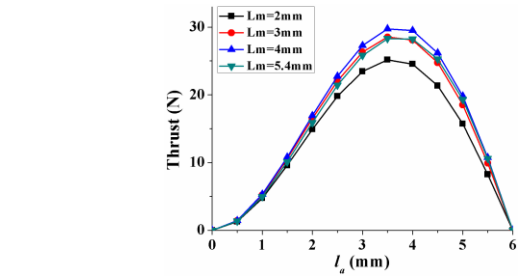

(a)

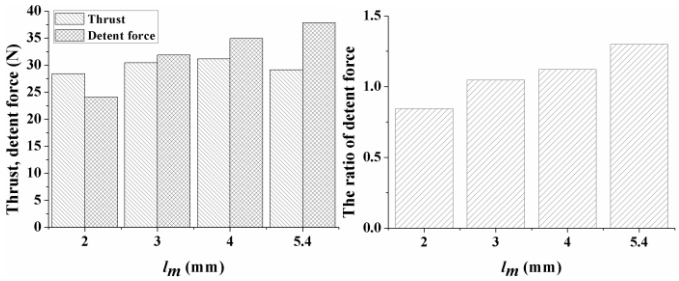

(b) (c)

Fig. 6. Results of thrust, detent force, and the ratio of detent force to thrust at various l_m. (a) Theoretical values of thrust. (b) Thrust and detent force based on 3-D FEM result when l_a is equal to 3.5mm. (c) Ratio of detent force to thrust based on 3-D FEM result when l_a is equal to 3.5mm.

V. Conclusion

In this paper, short armature core double-sided transverse flux type PMLSM was proposed. In addition, a theoretical design for a simple estimation of thrust in the designated dimension was created.

In the theoretical design, the authors focused on the thrust behavior in a one-core based configuration.

Although there were small differences between the estimation results and the 3-D FEM results due to the assumptions the authors made, a design point for high thrust and low detent force in the designated dimension was estimated using a simple calculation.

Future work will involve a design for high thrust and low detent force in 9 core-8 pole combination-based model. In the design, the effect of end force, core loss, and magnetic saturation will be analyzed. Also, further characterization of the prototype model through static and dynamic testing including thrust, thrust ripple, and positioning accuracy will be conducted.

References

[1] Zou. J. B, Wang. Q : “Fundamental Study on a Novel Transverse Flux Permanent Magnet Linear Machine”, Proceedings of the International Conference on Electrical Machines, pp. 2894-2898, 2008.

[2] Jo˜ao S. D. Garcia, Mauricio V. Ferreira da Luz, Jo˜ao Pedro A. Bastos, and Nelson Sadowski: “Transverse flux machine : what for? ”, IEEE Multidisciplinary Engineering Education Magazine, Vol. 2,No. 1, pp. 4-6, March 2007.

[3] J. Jung, J. Hong, and Y. Kim : “Characteristic Analysis and Comparison of IPMSM for HEV According to Pole and Slot Combination”, Vehicle Power and Propulsion Conference, VPPC 2007. IEEE, pp. 778-783, 2007.

[4] Krishnan Ramu : “Permanent Magnet Synchronous and Brushless DC Motors”, CRC Press/Taylor & Francis, 2009.

[5] Jacek F. Gieras, Zbigniew J. Piech : “Linear synchronous motors: transportation and automation systems”, CRC Press, 1999.